

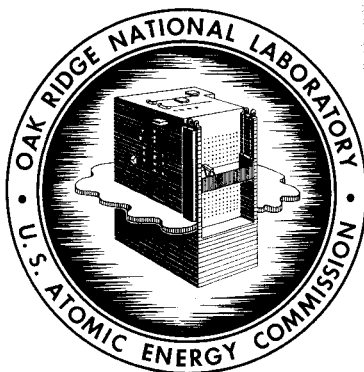
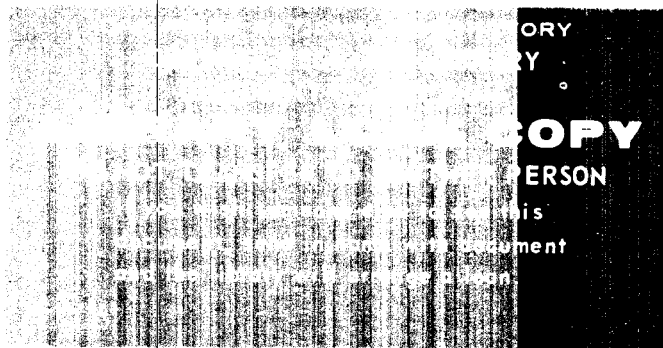


3 4456 0515836 1

ORNL-4211  
UC-34 - Physics

SHIELDING CALCULATIONS FOR A 400-MeV  
LINEAR ELECTRON ACCELERATOR

R. G. Alsmiller, Jr.  
J. Barish  
R. T. Boughner  
W. W. Engle



**OAK RIDGE NATIONAL LABORATORY**  
operated by  
**UNION CARBIDE CORPORATION**  
for the  
**U.S. ATOMIC ENERGY COMMISSION**

Printed in the United States of America. Available from Clearinghouse for Federal  
Scientific and Technical Information, National Bureau of Standards,  
U.S. Department of Commerce, Springfield, Virginia 22151  
Price: Printed Copy \$3.00; Microfiche \$0.65

LEGAL NOTICE

This report was prepared as an account of Government sponsored work. Neither the United States, nor the Commission, nor any person acting on behalf of the Commission:

- A. Makes any warranty or representation, expressed or implied, with respect to the accuracy, completeness, or usefulness of the information contained in this report, or that the use of any information, apparatus, method, or process disclosed in this report may not infringe privately owned rights; or
- B. Assumes any liabilities with respect to the use of, or for damages resulting from the use of any information, apparatus, method, or process disclosed in this report.

As used in the above, "person acting on behalf of the Commission" includes any employee or contractor of the Commission, or employee of such contractor, to the extent that such employee or contractor of the Commission, or employee of such contractor prepares, disseminates, or provides access to, any information pursuant to his employment or contract with the Commission, or his employment with such contractor.



3 4456 0515836 1

ORNL-4211

Contract No. W-7405-eng-26

Neutron Physics Division

## SHIELDING CALCULATIONS FOR A 400-MeV LINEAR ELECTRON ACCELERATOR

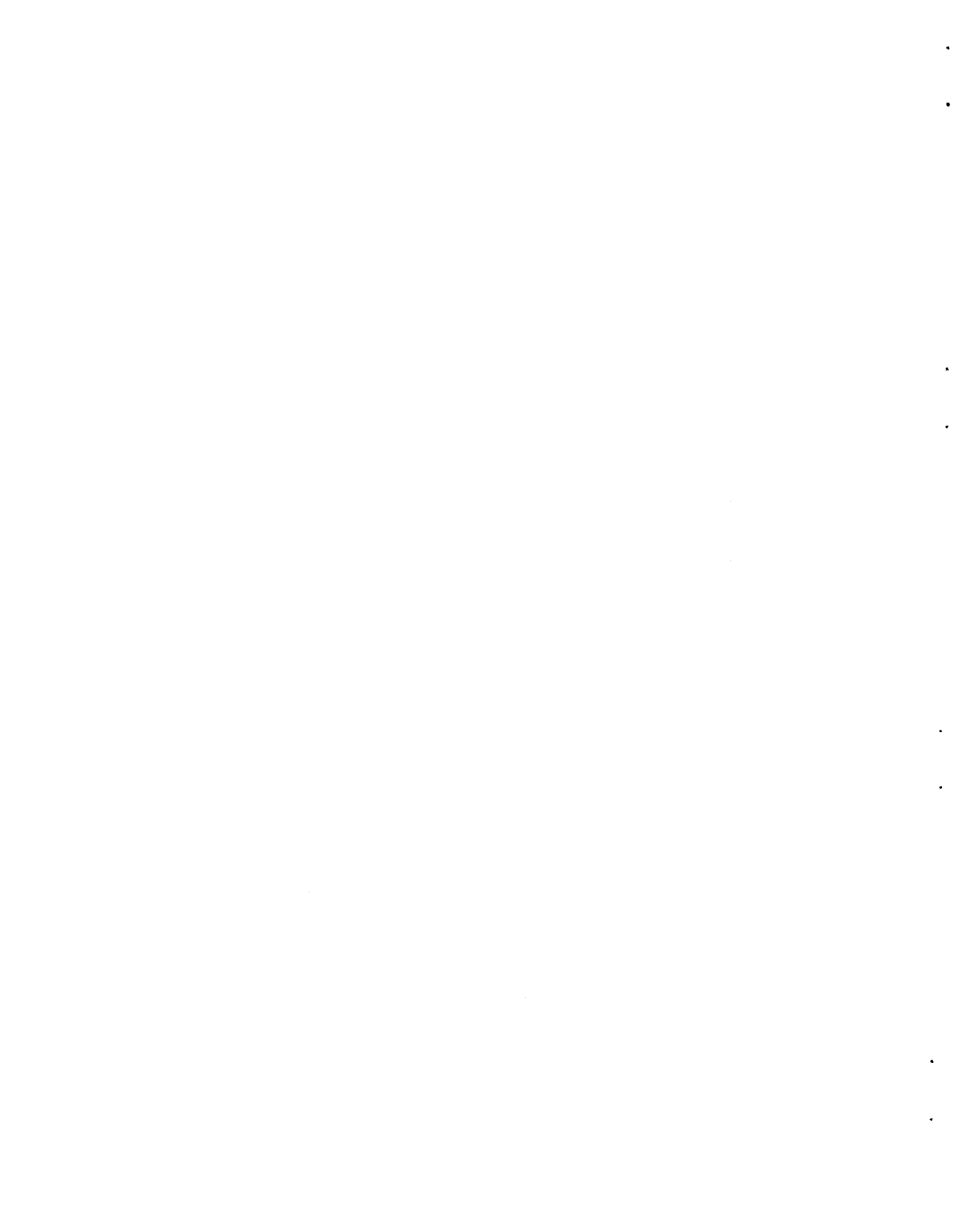
R. G. Alsmiller, Jr., J. Barish,\*

R. T. Boughner, and W. W. Engle\*

\*Computing Technology Center, Union Carbide Corporation, Oak Ridge,  
Tennessee.

JANUARY 1968

OAK RIDGE NATIONAL LABORATORY  
Oak Ridge, Tennessee  
operated by  
UNION CARBIDE CORPORATION  
U. S. ATOMIC ENERGY COMMISSION



ACKNOWLEDGMENT

We thank F. S. Alsmiller for helpful discussions concerning many phases of the work and F. R. Mynatt for his help in understanding the discrete ordinates calculations.

.

.

.

.

.

.

.

.

## TABLE OF CONTENTS

	<u>Page No.</u>
Abstract.....	1
1. INTRODUCTION.....	2
2. ELECTRON-PHOTON CASCADE.....	2
3. PHOTONEUTRON PRODUCTION.....	5
4. PARTICLE TRANSPORT.....	9
a. Straighthead Approximation.....	10
b. Straighthead Approximation Coupled with a Low- Energy Discrete Ordinates Calculation.....	15
c. Straighthead Approximation Coupled with a Monte Carlo Calculation.....	20
5. DOSE CALCULATION.....	22
6. RESULTS AND CONCLUSIONS.....	23
APPENDIX I .....	36
References .....	44



## SHIELDING CALCULATIONS FOR A 400-MeV LINEAR ELECTRON ACCELERATOR

R. G. Alsmiller, Jr., J. Barish,\*  
R. T. Boughner, and W. W. Engle\*

Abstract

Shielding calculations for a linear electron accelerator may conveniently be divided into four parts: 1) the electron-photon cascade, 2) photoneutron production, 3) particle transport through the shield, and 4) the conversion of particle current leaving the shield to dose. Calculations in each of these categories have been carried out to aid in the design of the transverse shield of a 400-MeV linear electron accelerator. In particular, neutron-transport calculations, which are carried out using three approximation methods, 1) the straightahead approximation, 2) the straightahead approximation coupled with a low-energy discrete ordinates calculation, and 3) the straightahead approximation coupled with a Monte Carlo calculation, are presented and compared. Shields composed of silicon dioxide and silicon dioxide with 10% water by weight are considered.

---

\* Computing Technology Center, Union Carbide Corporation, Oak Ridge, Tennessee.

## 1. INTRODUCTION

A series of calculations has been carried out to aid in the design of the transverse shield for a 400-MeV linear accelerator. While the calculations refer specifically to an electron accelerator of this energy, the electron-photon cascade calculations and the neutron transport through the shield have been carried out using several different approximations, and the intercomparison of the results obtained in these various approximations have general implications.

When a high-energy electron strikes the walls of the accelerator, an electron-photon cascade develops. The photons of the cascade interact with the nuclei in the walls and produce photoneutrons which must be shielded against. Shielding calculations for an electron accelerator may conveniently be divided into four parts: 1) the electron-photon cascade, 2) photoneutron production, 3) particle transport through the shield, and 4) the conversion of the particle current leaving the shield to dose. The calculations performed in each of these categories are described in sections 2, 3, 4, and 5, respectively. The results are presented and discussed in section 6.

## 2. ELECTRON-PHOTON CASCADE

A computer code for the study of the longitudinal and lateral development of the electron-photon cascade induced in matter by high-energy electrons has been written by C. D. Zerby and H. S. Moran.<sup>1-3</sup> Using this code the photon track length, which is needed to calculate the photoneutrons produced by the cascade, has been calculated for the case of 400-MeV electrons normally incident on an infinite slab of copper. This gives, of course,

only an approximation to the actual track length in the accelerator wall, but for the high-energy photons, which are of primary interest here, it is perhaps a reasonable approximation.

The calculated track length,  $T$ , is shown as a function of photon energy,  $E_\gamma$ , in Fig. 1. In the figure the solid histogram shows the results given by the Monte Carlo code and the solid curve drawn through the histogram gives the values which have been used in all subsequent calculations in this paper. Also shown in the figure for comparison purposes is the track length (solid curve below  $E_\gamma = 280$  MeV and dashed curve above  $E_\gamma = 280$  MeV) given by the often-used approximate expression,<sup>4</sup>

$$T(E_o, E_\gamma) = 0.572 \frac{E_o}{E_\gamma^2} X_o ,$$

where

$E_o$  = electron energy,

$E_\gamma$  = photon energy,

$X_o$  = radiation length.

The approximate track length is in very good agreement with the Monte Carlo results for photon energies of less than 280 MeV but becomes significantly different from the Monte Carlo results at higher photon energies.

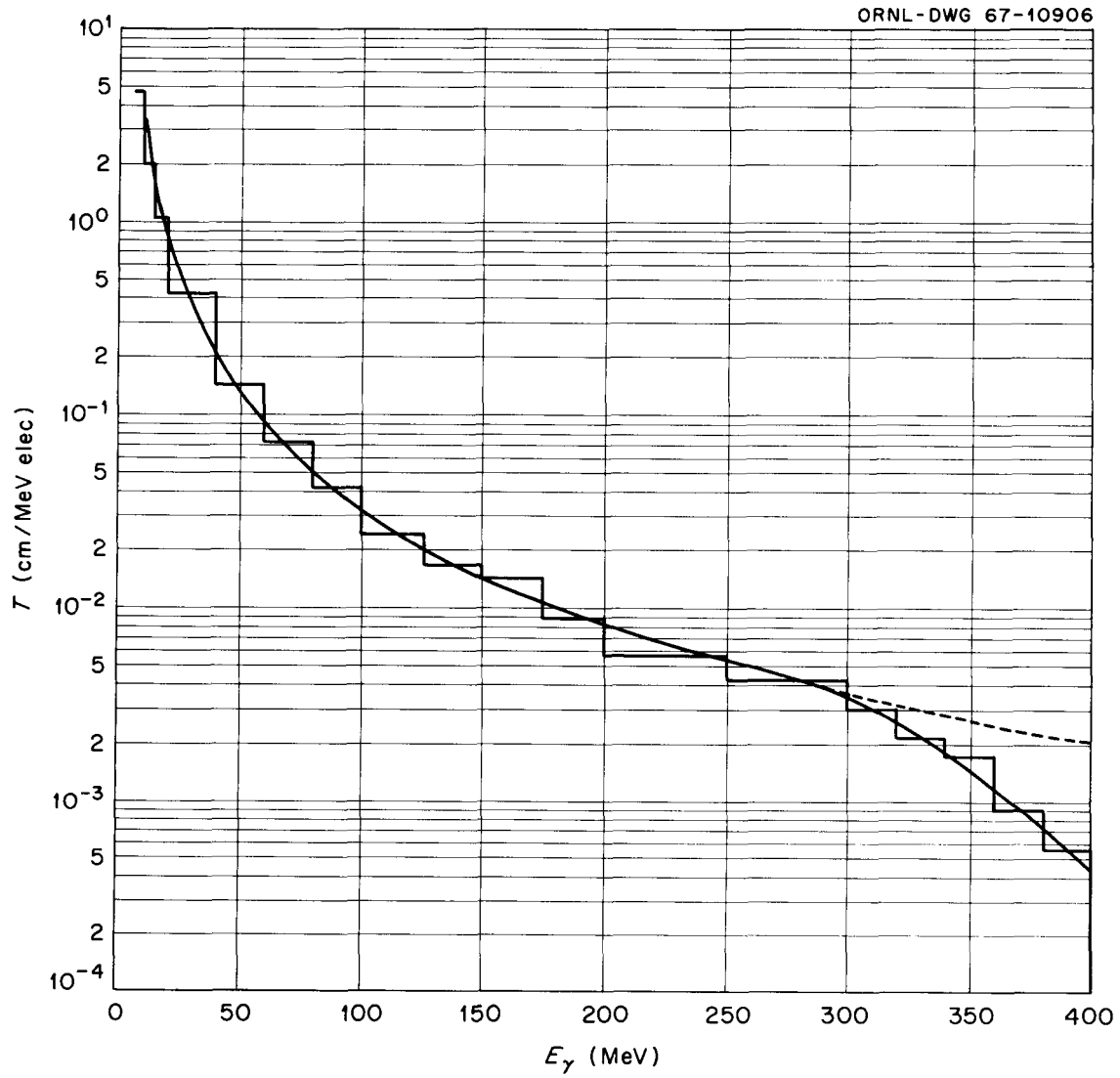


Fig. 1. Photon Track Length 400 MeV Electrons in Cu.

## 3. PHOTONEUTRON PRODUCTION

The energy and angular distribution of the neutrons produced by the cascade may be calculated from the equation

$$N_o(E, \cos\theta) = \int_0^E T(E_o, E_\gamma) n \frac{d\sigma}{dEd\Omega} (E_\gamma, E, \cos\theta) dE, \quad (3.1)$$

where

$E$  = kinetic energy in the laboratory system;

$\cos\theta$  = cosine of the angle defining neutron emission with respect to the direction of the incident electron. (The assumption is being made that the lateral spread of the cascade may be neglected so that the cosine of the angle defining neutron emission with respect to the direction of the photon in  $\frac{d\sigma}{dEd\Omega}$  may be equated with the cosine of the angle defining neutron emission with respect to the direction of the incident electron.)

$n$  = number density of targets;

$\frac{d\sigma}{dEd\Omega} (E_\gamma, E, \cos\theta)$  = differential cross section in the laboratory system for the production of neutrons by the collision of a photon of energy  $E_\gamma$  with a nucleus. (When integrated over all energies and angles,  $\frac{d\sigma}{dEd\Omega}$  gives not the total cross section for photon-nucleus collision but rather this total cross section multiplied by the average number of neutrons emitted per collision.)

$N_0(E, \cos\theta)$  = the number of neutrons per unit energy range per unit solid angle produced by the electron-photon cascade from an electron of energy  $E_0$ .

The differential cross section for photoneutron production is not well known and cannot readily be calculated. By introducing many *ad hoc* assumptions and utilizing earlier work by J. S. Levinger<sup>5</sup> and D. N. Olson,<sup>6</sup> H. De Staebler, Jr.<sup>7</sup> has obtained an estimate of this differential cross section. The cross section used in this paper has been calculated using all of the assumptions and parameters of De Staebler. Since the many approximations used and the choice of parameters in copper are discussed in detail in the paper by De Staebler,<sup>7</sup> only the final results will be given here.

In the approximation being used,  $\frac{d\sigma}{dE d\Omega}$  is composed of two terms: one which arises from the absorption of a photon by a neutron-proton pair, that is, by a "quasi-deuteron" in the nucleus, and one which arises from pion production and reabsorption in the same nucleus, that is, a pion is formed as a result of a photon-nucleon collision in the nucleus and the pion is reabsorbed by two nucleons before it escapes from the nucleus.\* If these two terms are denoted by  $\left. \frac{d\sigma}{dE d\Omega} \right|_{\text{QD}}$  and  $\left. \frac{d\sigma}{dE d\Omega} \right|_{\pi}$ , respectively, the photoproduction cross section may be calculated from the equations<sup>†</sup>:

$$\frac{d\sigma}{dE d\Omega} = \left. \frac{d\sigma}{dE d\Omega} \right|_{\text{QD}} + \left. \frac{d\sigma}{dE d\Omega} \right|_{\pi}, \quad (3.2)$$

---

\* A third term that arises from the recoil nucleon following pion production from a photon-nucleon collision should, in principle, be present. This term, however, is zero at  $\cos\theta = 90^\circ$ , which is the only case actually used in this paper.

† Some of the details of deriving these final equations, which are not given explicitly by De Staebler, are given in Appendix I.

$$\left. \frac{d\sigma}{dE d\Omega} \right|_{QD} = A \frac{\sigma_D(E_\gamma)}{4\pi} J_D(E, \cos\theta) \delta \left[ E_\gamma - \frac{2mE}{\cos\theta \sqrt{E(E+2m)} + m - E} \right] \quad (3.3)$$

$$J_D(E, \cos\theta) = \sqrt{2} \frac{\sqrt{E(E+2m)}}{\sqrt{E}} \frac{\sqrt{\cos\theta [E(E+2m)]^{\frac{1}{2}} + E + m}}{\cos\theta [E(E+2m)]^{\frac{1}{2}} - E + m},$$

$$\left. \frac{d\sigma}{dE d\Omega} \right|_{\pi} = 0.8 A \frac{\sigma_{\pi}(E_\gamma)}{4\pi} J_{\pi}(E, \cos\theta) \delta \left[ E_\gamma - \frac{2mE - \frac{1}{2} m_{\pi}^2}{\cos\theta \sqrt{(2E + m_{\pi})(2E - m_{\pi})} + m - 2E} \right]$$

$$J_{\pi}(E, \cos\theta) = \frac{2\sqrt{(2E + m_{\pi})(2E - m_{\pi})}}{Q(E_\gamma) [\cos\theta \sqrt{(2E + m_{\pi})(2E - m_{\pi})} + m - 2E]} \quad (3.4)$$

$$Q(E_\gamma) = \frac{[m^2 E_\gamma^2 - m m_{\pi}^2 E_\gamma + \frac{1}{4} m_{\pi}^4 - m^2 m_{\pi}^2]^{\frac{1}{2}}}{m(2E_\gamma + m)},$$

where

$A$  = atomic weight

$\sigma_D$  = total cross section for dissociation of a deuteron

$m$  = nucleon mass

$\sigma_{\pi}$  = total cross section for pion production in photon-nucleon collision

$m_{\pi}$  = pion mass

The photoneutron emission spectrum at  $90^\circ$  from 400-MeV electrons in copper, calculated using Eqs. 3.1 through 3.4, is shown in Fig. 2. The functions  $N_{OD}$  and  $N_{O\pi}$  are obtained by using Eqs. 3.3 and 3.4 separately in Eq. 3.1, so

$$N_O = N_{OD} + N_{O\pi} \quad (3.5)$$

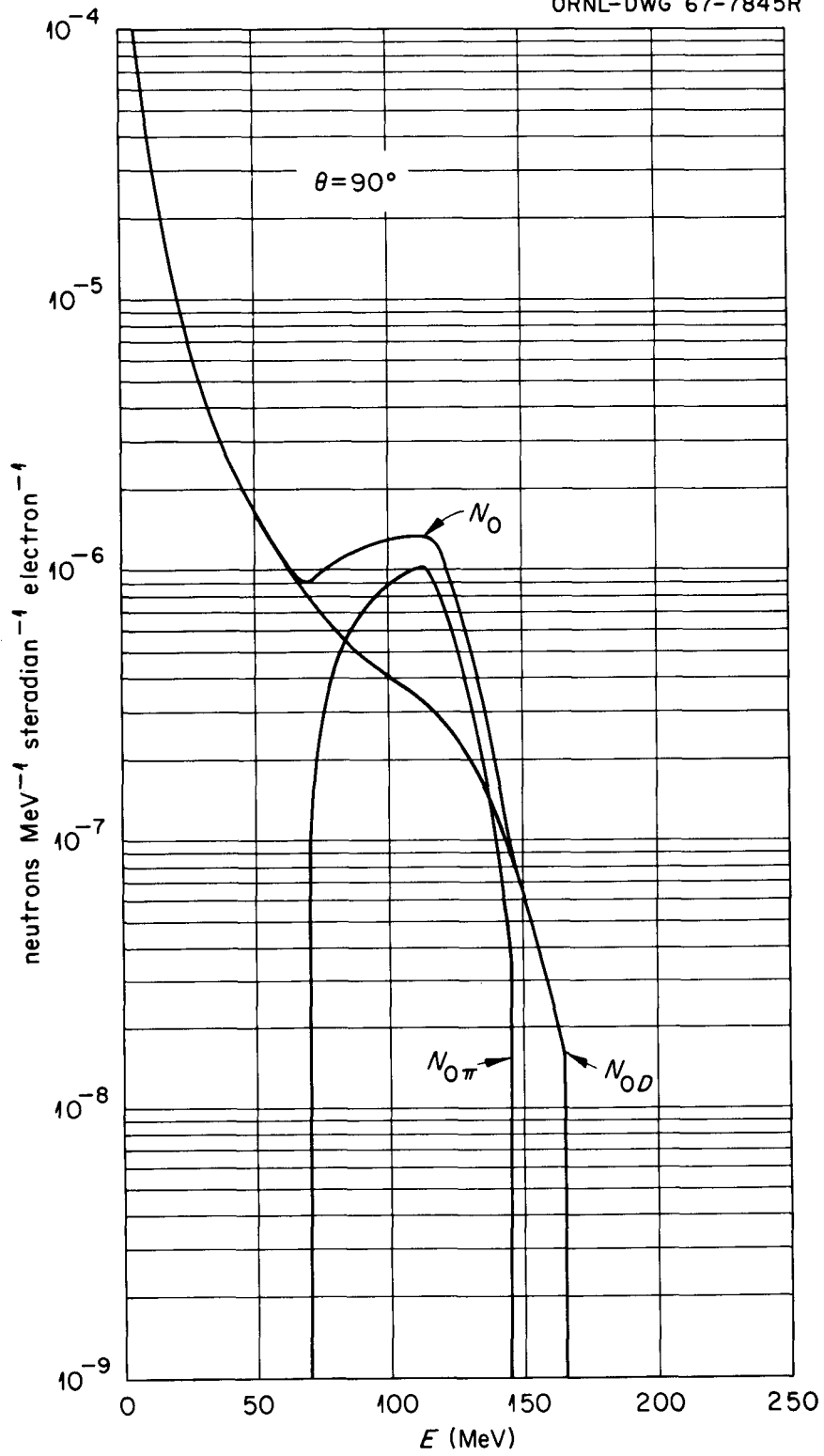


Fig. 2. Photoneutron Spectrum 400-MeV Electrons in Cu.

In the case shown in the figure,  $N_{O\pi}$  contributes appreciably to  $N_O$  over a significant part of the energy range. The high-energy cutoff in the photoneutron spectrum arises because the motion of the nucleons in the nucleus has been neglected.\*

#### 4. PARTICLE TRANSPORT

The transverse shield of a linear accelerator may be visualized as being roughly cylindrical in shape with the accelerator tube along the axis of the cylinder. In principle, electrons of varying energy strike the accelerator tube all along its length and the geometry that should be considered is that of a line source with both the energy and angular distributions of the neutrons from the source varying as a function of position along the line. Rather than treat this general problem, it is assumed here that only high-energy electrons are of interest and that all high-energy electrons may be assumed to strike the accelerator tube at nearly the same point. The electron-photon cascade, which develops when a high-energy electron enters matter, and the resulting photoproduction take place over distances that are very small compared to the shield thicknesses of interest, and thus to a reasonable approximation the photoneutrons may be assumed to emanate from a point. Furthermore, it is unlikely that high-energy electrons will strike the walls of the accelerator tube at angles which are very different from zero degrees, so it will be assumed that photoneutron emission with respect to the direction of the incident electron may be equated with photoneutron emission with respect to the accelerator axis. The minimum shield thickness will therefore be in the direction of those neutrons emitted with  $\cos\theta = 90^\circ$ .

---

\* A calculation of  $N_{OD}$ , which includes this motion, has recently been carried out by J. L. Matthews.<sup>8,9</sup>

The geometry that is considered here is that of a point source of neutrons on the axis of the accelerator. Because of the approximations which are made in the transport equations, only neutrons emitted at a specific angle enter into the calculations, and results are presented only for the case of neutron emission in the direction of minimum shield thickness. Shields composed of silicon dioxide and silicon dioxide plus water are considered.

When a high-energy neutron enters matter, a cascade composed of neutrons, protons, and photons will develop. At the neutron energies of interest here, however, the protons and photons will be predominantly of low energy and will contribute little to the cascade, so in general only neutron transport is considered. In the remainder of this section, the various approximations that are used to describe the neutron transport through the shield are discussed. In conjunction with one of the transport methods (see section 4.b), photon production and transport are treated.

a. Straightahead Approximation

In this approximation it is assumed that neutron emission following either elastic or nonelastic neutron-nucleus collisions take place only in the direction of the incident neutron. The energy distribution of the neutron emitted in the forward direction must be specified. This energy distribution may be obtained by integrating the energy-angle distribution of the emitted neutrons over all angles or by integrating over some cone in the forward direction; that is, one may simply neglect those particles emitted at large angles. Throughout this paper the energy distributions are specified by integrating over all angles.

In addition to the straightahead approximation, it will also be assumed that elastic collisions between neutrons and heavy nuclei, that is, nuclei heavier than hydrogen, may be treated in a continuous slowing-down approximation.

Under these circumstances, the neutron transport equation when there is a point source of neutrons may be written

$$\frac{\partial}{\partial r} r^2 N(r, E) + \left\{ \sum_i n_i [\sigma_{Ii}(E)(1-\delta_{iH}) + \sigma_{Ei}(E) \delta_{iH}] \right\} r^2 N(r, E) - \frac{\partial}{\partial E} [S(E) r^2 N(r, E)] \quad (4.1)$$

$$= \sum_i \int_E^{E_{MAX}} [F_i(E', E) n_i \sigma_{Ii}(E')(1-\delta_{iH}) + G_i(E', E) n_i \sigma_{Ei}(E') \delta_{iH}] r^2 N(r, E') dE' ,$$

where

$r$  = radial coordinate measuring depth into the shield from the point source;

$N(r, E)$  = neutron current per unit energy range, that is, the number of neutrons per unit energy range crossing unit area at a depth  $r$  in the shield. (In the approximation being used, the neutron velocity at any point in the shield is in the radial direction.)

$n_i$  = number density of nuclei of type  $i$  in the shield;

$\sigma_{Ii}(E)$  = nonelastic cross section for the collision of a neutron of energy  $E$  with a nucleus of type  $i$ ;

$\delta_{iH}$  = one if  $i$  is hydrogen and zero otherwise;

$\sigma_{Ei}(E)$  = elastic cross section for the collision of a neutron of energy  $E$  and a nucleus of type  $i$ ;

$S(E)$  = energy loss per unit distance that a neutron undergoes because of elastic collisions with nuclei other than hydrogen;

$F_i(E',E)$  = number of neutrons per unit energy range produced by the nonelastic collision of a neutron of energy  $E'$  with a nucleus of type  $i$ ;

$G_i(E',E)$  = number of neutrons per unit energy range produced by the elastic collision of a neutron of energy  $E'$  with a nucleus of type  $i$ .

The boundary condition on Eq. 4.1 is that the intensity  $I$ , defined by

$$I(r,E) = r^2 N(r,E) , \quad (4.2)$$

reduce to the energy distribution per unit solid angle of the source when  $r$  goes to zero. Since in general this energy distribution will be a function of the direction in which the particles are emitted, the solution will be parameterized by the direction of emission.

In order to obtain a numerical solution to Eq. 4.1, a large amount of physical data is required. The cross sections for nonelastic neutron-silicon and neutron-oxygen collisions at energies greater than 25 MeV were taken from the calculations of Bertini.<sup>10,11</sup> Since Bertini does not report data for silicon, the data used were obtained by interpolation. The cross sections for neutron-silicon and neutron-oxygen nonelastic collisions below 25 MeV were taken from the data compilation of Irving.<sup>12</sup> In some instances when data for silicon were not available, data for aluminum were used. The cross sections for neutron-hydrogen elastic collisions below 25 MeV were taken from the compilation of Irving<sup>12</sup> and above 25 MeV from the compilation of Bertini.<sup>13</sup>

The energy distributions of neutrons emitted from neutron-silicon and neutron-oxygen nonelastic collisions above 25 MeV were taken from the calculations of Bertini.<sup>10,11</sup> These distributions were obtained by integrating the energy-angle distributions of both the cascade and evaporation neutrons over all angles. The energy distributions of neutrons from neutron-silicon and neutron-oxygen nonelastic collisions below 25 MeV were assumed to be of the form

$$F_i(E', E) = \frac{E}{T_i^2(E')} e^{-\frac{E}{T_i(E')}} \quad E < E' , \quad (4.3)$$

and the functions  $T_i(E')$  were calculated from the equations used by Dresner in his evaporation code.<sup>14</sup> Equation 4.3 gives a neutron multiplicity which is very nearly unity and which is roughly in agreement with the results given by the Dresner evaporation code.

The energy distributions of the neutrons from neutron-hydrogen elastic collisions were obtained by transforming the angular distribution in the center-of-momentum system to the energy-angle distribution in the laboratory system and integrating over all angles.<sup>15</sup> The angular scattering distribution in the center-of-momentum system was taken to be isotropic for incident neutron energies of less than 25 MeV, and above this energy it was taken from the analytic fits given by Bertini to the measured distributions.

The stopping power  $S$  may be defined by the equation

$$S(E') = \sum_i n_i \sigma_{Ei}(E') E' \left[ \log \frac{E'}{E} \right]_i \quad (4.4)$$

$$\left[ \log \frac{E'}{E} \right]_i = \int_0^{E'} G_i(E', E) \log \frac{E'}{E} dE ,$$

where all of the symbols have the definitions given previously and the sum over  $i$  does not include hydrogen since neutron-hydrogen collisions have been explicitly introduced into Eq. 4.1. At neutron energies of several MeV and below, the elastic scattering cross sections contain resonances, and these resonances cause  $S(E')$ , defined by Eq. 4.4, to be a very rapidly varying function of energy. To avoid the numerical difficulties associated with this rapid variation, a smoothing procedure was used at the lower energies. The distance  $R$  that a neutron will travel in going from an energy  $E$  to some low energy  $E_c$  may be written

$$R(E) = \int_{E_c}^E \frac{dE'}{S(E')} . \quad (4.5)$$

To obtain a smoothly varying stopping power,  $R(E)$ , calculated using Eqs. 4.3 and 4.4, was assumed to be of the form

$$R(E) = e^{\sum_{j=0}^8 a_j E^j} , \quad (4.6)$$

and the coefficients,  $a_j$ , were determined by the method of least squares. Once the coefficients were determined, the stopping power was calculated from the equation

$$\frac{1}{S(E)} = \left[ \sum_{j=0}^8 j a_j E^{j-1} \right] e^{\sum_{j=0}^8 a_j E^j} . \quad (4.7)$$

The elastic scattering cross sections and the center-of-momentum angular distributions, which were needed to obtain the energy distributions in Eq. 4.4, were taken from the compilation of Irving.<sup>12</sup> The smoothing procedure discussed above was used at energies of less than 26 MeV. Above this energy,  $S(E)$  is slowly varying and could be used directly.

Calculations using the straightahead approximation have been carried out for neutron energies greater than 0.5 MeV. There is, of course, little justification for using the approximation at such low energies, and it is to be expected that a considerable overestimate of the low-energy neutron flux and the resulting dose will be obtained when this method is used. In the next section an approximation method, which retains the straightahead approximation at the higher energies but treats the low-energy neutron transport more realistically, is described.

b. Straightahead Approximation Coupled with a Low-Energy Discrete Ordinates Calculation

The transport of low-energy neutrons has been intensively studied for many years. There is presently available a discrete ordinates code which will solve the neutron transport equation with anisotropic scattering in one space dimension for neutron energies of less than 14.9 MeV provided the neutron source is known.<sup>16</sup> In the approximation to be described in this section, the straightahead approximation is used to transport the high-energy (>14.9 MeV) neutrons, and the calculated high-energy neutron flux is used to construct a source of low-energy neutrons that is used in conjunction with the discrete ordinates code.

The neutron transport equation may be written as

$$\begin{aligned} & \vec{\Omega} \cdot \nabla \phi(\vec{r}, E, \vec{\Omega}) + \sum_i n_i [\sigma_{Ei}(E) + \sigma_{Ii}(E)] \phi(\vec{r}, E, \vec{\Omega}) \\ &= \sum_i \int_E^{E_{MAX}} \{F_i(E', E, \vec{\Omega}' \cdot \vec{\Omega}) n_i \sigma_{Ii}(E') \\ &+ G_i(E', E, \vec{\Omega}' \cdot \vec{\Omega}) n_i \sigma_{Ei}(E')\} \phi(\vec{r}, E', \vec{\Omega}') dE' d\Omega' \quad , \end{aligned} \quad (4.8)$$

where

$\vec{r}$  = position vector,

$\vec{\Omega}$  = unit vector in the direction of the momentum,

$\phi(\vec{r}, E, \vec{\Omega})$  = angular flux of neutrons per unit energy range,

$F_i(E', E, \vec{\Omega}' \cdot \vec{\Omega})$  = the number of neutrons per unit energy range per unit solid angle produced at the energy E and in the direction  $\vec{\Omega}$  when a neutron with energy E' going in the direction  $\vec{\Omega}'$  undergoes a nonelastic collision with a nuclei of type i,

$G_i(E', E, \vec{\Omega}' \cdot \vec{\Omega})$  = the number of neutrons per unit energy range per unit solid angle produced at the energy E and in the direction  $\vec{\Omega}$  when a neutron with energy E' going in the direction  $\vec{\Omega}'$  undergoes an elastic collision with a nuclei of type i.

If Eq. 4.7 is rewritten in the form

$$\begin{aligned} \vec{\Omega} \cdot \nabla \phi(\vec{r}, E, \vec{\Omega}) + \sum_i n_i [\sigma_{Ei}(E) + \sigma_{Ii}(E)] \phi(\vec{r}, E, \vec{\Omega}) \\ = \sum_i \int_E^{14.9} \{F_i(E', E, \vec{\Omega}' \cdot \vec{\Omega}) n_i \sigma_{Ii}(E') \\ + G_i(E', E, \vec{\Omega}' \cdot \vec{\Omega}) n_i \sigma_{Ei}(E')\} \phi(\vec{r}, E', \vec{\Omega}') dE' d\Omega' + S(\vec{r}, E, \vec{\Omega}), \end{aligned} \quad (4.9)$$

we have the equation which, when specialized to one space dimension, the discrete ordinates code will solve if  $S(\vec{r}, E, \vec{\Omega})$ , defined by

$$\begin{aligned}
S(\vec{r}, E, \vec{\Omega}) = \sum_i \int_{14.9}^{E_{\text{MAX}}} \{ & F_i(E', E, \vec{\Omega}' \cdot \vec{\Omega}) n_i \sigma_{Ii}(E') \\
& + G_i(E', E, \vec{\Omega}' \cdot \vec{\Omega}) n_i \sigma_{Ei}(E') \} \phi(\vec{r}, E', \vec{\Omega}') dE' d\Omega' ,
\end{aligned} \tag{4.10}$$

is known. To obtain an approximate expression for S in the case of a one-dimensional spherical geometry, it is assumed that the straightahead approximation is valid for neutron energies greater than 14.9 MeV, so

$$\phi(r, E, \vec{\Omega}_r \cdot \vec{\Omega}) = N(r, E) \frac{\delta(1 - \vec{\Omega}_r \cdot \vec{\Omega})}{2\pi} , \quad E > 14.9 \text{ MeV}, \tag{4.11}$$

where

$$\vec{\Omega}_r = \text{a unit vector in the radial direction.}$$

Furthermore, it is assumed that

$$F_i(E', E, \vec{\Omega}' \cdot \vec{\Omega}) = \frac{F_i(E', E)}{4\pi} \begin{array}{l} E' > 14.9 \text{ MeV} \\ E < 14.9 \text{ MeV} \end{array} \tag{4.12}$$

and

$$G_i(E', E, \vec{\Omega}' \cdot \vec{\Omega}) = G_i(E', E) \frac{\delta(1 - \vec{\Omega}' \cdot \vec{\Omega})}{2\pi} \begin{array}{l} E' > 14.9 \text{ MeV} \\ E < 14.9 \text{ MeV} \end{array} , \tag{4.13}$$

where  $F_i(E', E)$  and  $G_i(E', E)$  are the quantities defined in 4.a.

With these approximations the source S may be written

$$\begin{aligned}
S(r, E, \vec{\Omega}_r \cdot \vec{\Omega}) = \sum_i \int_{14.9}^{E_{\text{MAX}}} \{ & \frac{F_i(E', E)}{4\pi} n_i \sigma_{Ii}(E') \\
& + \frac{\delta(1 - \vec{\Omega}_r \cdot \vec{\Omega})}{2\pi} G_i(E', E) n_i \sigma_{Ei}(E') \} N(r, E') dE'
\end{aligned} \tag{4.14}$$

and may be calculated using the previously determined  $N(r,E)$ . Using this approximate source term in Eq. 4.9, in principle it is now possible to determine the flux per unit energy range of low-energy neutrons with the discrete ordinates code.

To avoid excessive computation and because the low-energy neutrons are of little interest at the beginning of the shield, Eq. 4.9 was actually solved for only  $r$  values greater than  $600 \text{ g/cm}^2$ . In order to do this, it was necessary, of course, to have an estimate of the flux at this  $r$ . This boundary condition was obtained by assuming the straightahead approximation to be valid at all energies for  $r \leq 600 \text{ g/cm}^2$ . The boundary condition used was

$$\begin{aligned} \phi(600, E, \vec{\Omega}_r \cdot \vec{\Omega}) &= N(600, E) \frac{\delta(1 - \vec{\Omega}_r \cdot \vec{\Omega})}{2\pi} & 0.5 \leq E \leq E_{\text{MAX}} \\ &= 0 & E < 0.5 \end{aligned} \quad (4.15)$$

since  $N(r,E)$  was not determined for  $E < 0.5$ .

The data that were used to calculate the source term are the same as those described in section 4.a. The data that were used in the discrete ordinates code were taken from the work of Joanou and Dudek.<sup>17</sup>

In calculating the dose and comparing the results, we shall be interested in the current per unit energy of the particles emerging from the shield and in the intensity. This poses a slight problem because at a given depth  $r$  in a shield of radius  $R$  ( $R > r$ ), the current per unit energy is different than it would be if the shield were of thickness  $r$ , and thus, in principle, to obtain the current of particles emerging from a shield, the complete calculation must be repeated for each shield thickness. To

avoid this difficulty here, it will be assumed that the current leaving a shield of thickness  $r$  may be approximated by the current in the positive  $r$  direction at a depth  $r$  in a shield of thickness  $R$ ; that is, the current leaving a shield of thickness  $r$  will be approximated by

$$J(r,E) = \int_0^{2\pi} \int_0^1 \phi(r,E, \vec{\Omega}_r \cdot \vec{\Omega}) \vec{\Omega}_r \cdot \vec{\Omega} d\Omega \quad E \leq 14.9 \text{ MeV} , \quad (4.16)$$

where  $\phi$  is the flux per unit energy at depth  $r$  in a shield of thickness  $R$ . Of course the only estimate one has at the higher energies is that given by the straightahead approximation. In the previous section, the intensity was defined to be the current per unit energy multiplied by  $r^2$ , and this definition will be retained with the proviso that only the current in the forward direction be used. Therefore,

$$\begin{aligned} I(r,E) &= r^2 J(r,E) & E \leq 14.9 \text{ MeV} \\ &= r^2 N(r,E) & E > 14.9 \text{ MeV} \end{aligned} \quad (4.17)$$

In addition to the neutrons that emerge from the shield, there will also be some photons that emerge. The contribution of these photons to the dose is not expected to be large, but in conjunction with the neutron transport approximation described above, an estimate of the gamma-ray flux leaving the shield has been obtained.

The gamma rays that emerge from the shield will be formed predominantly from neutron capture and neutron inelastic scattering. Because the neutron spectra in the shield are sharply peaked toward low energy and because of the lack of data on gamma production from neutron inelastic scattering, only the gamma rays arising from neutron capture are considered here. The neutron capture cross sections were taken from ref. 17 and the capture

photon spectra were taken from the Reactor Handbook.<sup>18</sup> It was assumed that the photon spectrum from neutron capture is a function of the nucleus but not of the energy of the neutron. The photons were transported using the same discrete ordinates code that was used for neutron transport. The photon source was calculated from the neutron flux obtained with the discrete ordinates code. In transporting the photons, account was taken of pair production, Compton scattering, and the photoelectric effect.

While the neutron transport method described in this section treats the low-energy transport realistically, the calculated flux at the low energies is still approximate because of the use of the straightahead approximation at the high energies. Furthermore, the only estimate of the neutron current per unit energy emerging from the shield at the higher energies is that given by the straightahead approximation, and thus appreciable error in the dose may arise from the approximate nature of the high-energy current. In the next section of this paper, an approximation method in which some of these difficulties are avoided will be described.

### c. Straightahead Approximation Coupled with a Monte Carlo Calculation

There is available a code written by Kinney<sup>19</sup> that will solve the neutron transport equation, Eq. 4.8, for neutron energies of less than approximately 400 MeV. In principle, this code could be used to obtain a complete solution to the neutron transport problem being considered. However, the code employs Monte Carlo methods and is not, at least in its present form, capable of yielding adequate statistical accuracy in the case of very thick shields. In this section, an approximation method is described whereby the straightahead approximation is used to transport the neutrons through the beginning of the shield and the Monte Carlo code is used to transport the neutrons through the last few collision mean free paths.

The Monte Carlo code has been described in detail elsewhere,<sup>19</sup> so only a few pertinent facts about the code will be included here. The code uses the intranuclear-cascade data of Bertini<sup>10</sup> to describe nonelastic neutron-nucleus collisions above 25 MeV and the compilation of Bertini<sup>13</sup> to describe neutron-proton collisions above 25 MeV. Below 25 MeV the data compilation of Irving<sup>12</sup> is used, and particle production from nonelastic collisions is obtained from the Dresner evaporation code.<sup>14</sup> In the Monte Carlo calculation aluminum data are used to represent silicon throughout.

The Monte Carlo code of Kinney will solve the neutron transport equation for an arbitrary incident neutron flux per unit energy range. In the present instance, to avoid statistics problems the straightahead approximation was used to obtain an estimate of the flux per unit energy range at a depth of 750 g/cm<sup>2</sup> in the shield, and this approximate flux was used in conjunction with the Monte Carlo code to estimate the flux at larger depths. One further approximation was made: The spherical shell through which the neutrons should be transported was approximated by a semi-infinite slab. The actual procedure used was to assume that the incident flux per unit energy to be used in the Monte Carlo code was given by

$$\Phi(z, E, \vec{\Omega}_z \cdot \vec{\Omega}) \Big|_{z=750 \text{ g/cm}^2} = \left[ r^2 N(r, E) \right]_{r=750 \text{ g/cm}^2} \frac{\delta(1 - \vec{\Omega}_z \cdot \vec{\Omega})}{2\pi}, \quad (4.18)$$

where

$z$  = a coordinate which measures depth into the slab,

$\vec{\Omega}_z$  = a unit vector in the  $z$  direction,

and  $N(r, E)$  is the quantity calculated in section 4.a; that is, in the Monte Carlo calculations normal incidence on a slab shield was considered. In the Monte Carlo calculations it is possible to treat several shield thicknesses simultaneously; that is, it is possible to calculate the flux at a

depth  $z$  when the shield is of thickness  $Z$ , and this is the quantity that has been calculated.

In calculating the dose and comparing the results we are interested in the current per unit energy of the particles leaving the shield and in the intensity. The current is calculated from the equation

$$J(\mathbf{z}, E) = \int_0^{2\pi} \int_0^1 \phi(\mathbf{z}, E, \vec{\Omega}_z \cdot \vec{\Omega}) \vec{\Omega}_z \cdot \vec{\Omega} d\Omega \quad . \quad (4.19)$$

Because of the slab approximation it is not entirely clear how to define an intensity which is comparable with that defined in the previous methods. A reasonable definition would seem to be that the intensity is equal to the current, that is,

$$I(r, E) = J(\mathbf{z}, E) \Big|_{z=r} \quad , \quad (4.20)$$

and this is the basis on which comparisons with the other calculations will be made.

## 5. DOSE CALCULATION

The dose has been estimated from the particle current emerging from the shield by using current-to-dose conversion factors. Once the current is known, the dose is calculated from the equation

$$D(r) = \int_{E_T}^{E_{MAX}} J(r, E) C(E) dE \quad , \quad (5.1)$$

where

$E_T$  = thermal energy

$C(E)$  = current-to-dose conversion factor.

The current-to-dose conversion factors for neutrons were taken from Snyder and Neufeld<sup>20</sup> (<0.5 MeV), Irving *et al.*<sup>21</sup> (0.5 to 60 MeV), and Zerby and Kinney<sup>22</sup> (>60 MeV). The conversion factors used in all cases were those corresponding to the maximum dose for normally incident neutrons on semi-infinite tissue slabs. The current-to-dose conversion factors for photons were taken from the work of Henderson.<sup>23</sup> It must of course be understood that the dose estimates obtained using these conversion factors are very approximate. In particular, the use of the conversion factors corresponding to normal incidence rather than to isotropic incidence is arbitrary. All of the doses calculated here would be approximately a factor of two higher if the isotropic conversion factors were used.

## 6. RESULTS AND CONCLUSIONS

Calculations have been carried out for shields composed of silicon dioxide and silicon dioxide with 10% water by weight. In all cases the density of the shield material was taken to be 1.8 g/cm<sup>3</sup>.

The results for the spectrum shown in Fig. 2 incident on the silicon dioxide shield are shown in Figs. 3-5. In Figs. 3 and 4 the neutron intensities (see definition Eqs. 4.2, 4.17, and 4.20) obtained in each approximation at a depth of 1000 g/cm<sup>2</sup> are compared, while in Fig. 5 the doses as a function of depth obtained in the various approximations are compared. The corresponding results for the shield composed of silicon dioxide and water are shown in Figs. 6-8.

In Figs. 3 and 6 the lowest energy point shown for the discrete ordinates calculation is 0.01 MeV. The spectrum, of course, does not stop at this energy but continues to increase very rapidly with decreasing energy

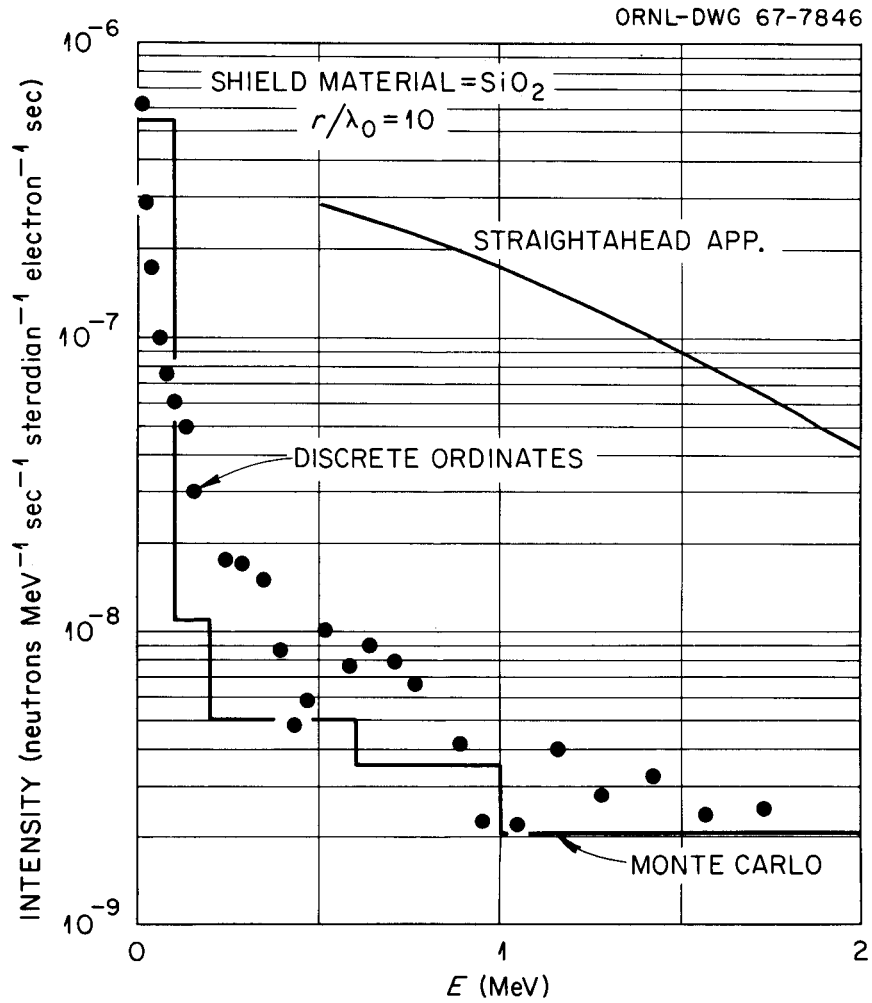


Fig. 3. Neutron Intensity vs Energy.

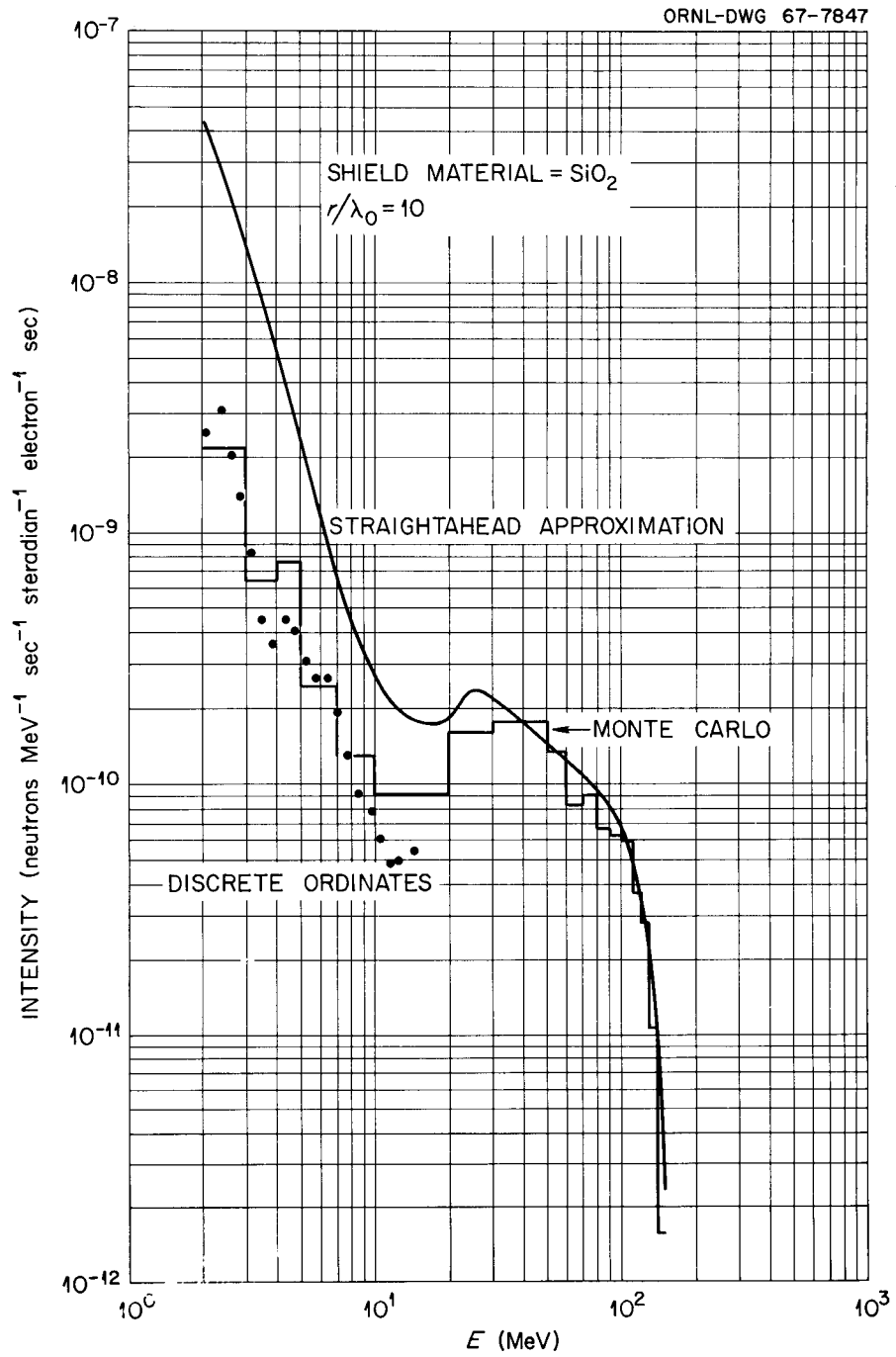


Fig. 4. Neutron Intensity vs Energy.

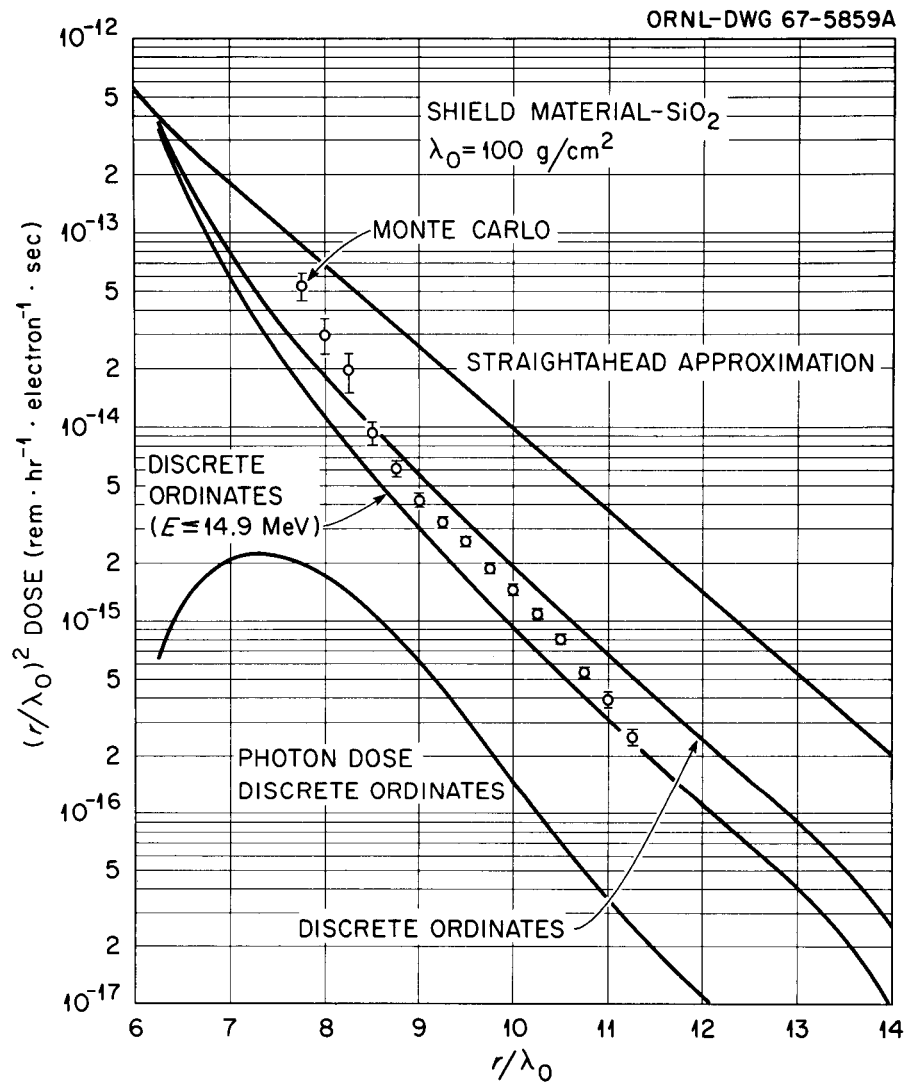


Fig. 5.  $\left(\frac{r}{\lambda_0}\right)^2$  Dose vs Radius.

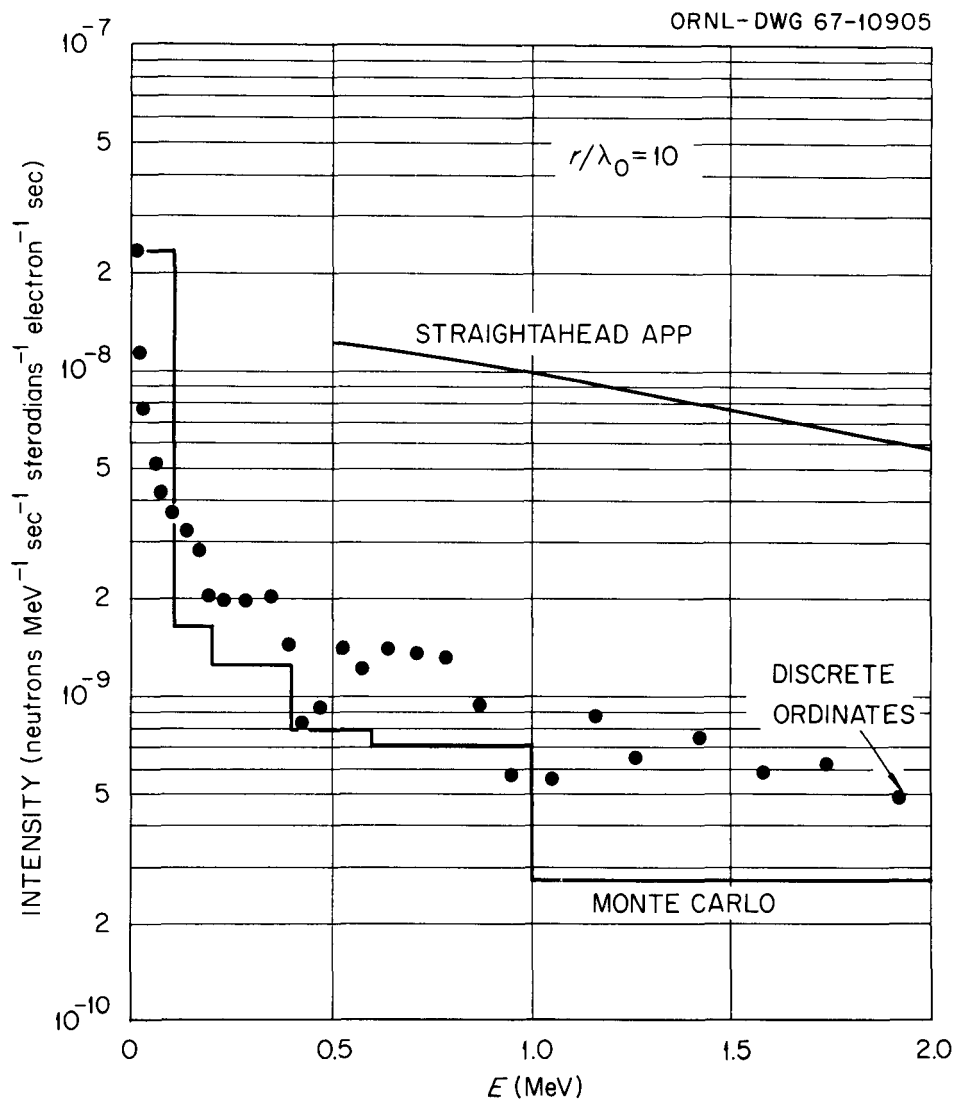


Fig. 6. Neutron Intensity vs Energy Shield Material =  $\text{SiO}_2$  with 10%  $\text{H}_2\text{O}$ .

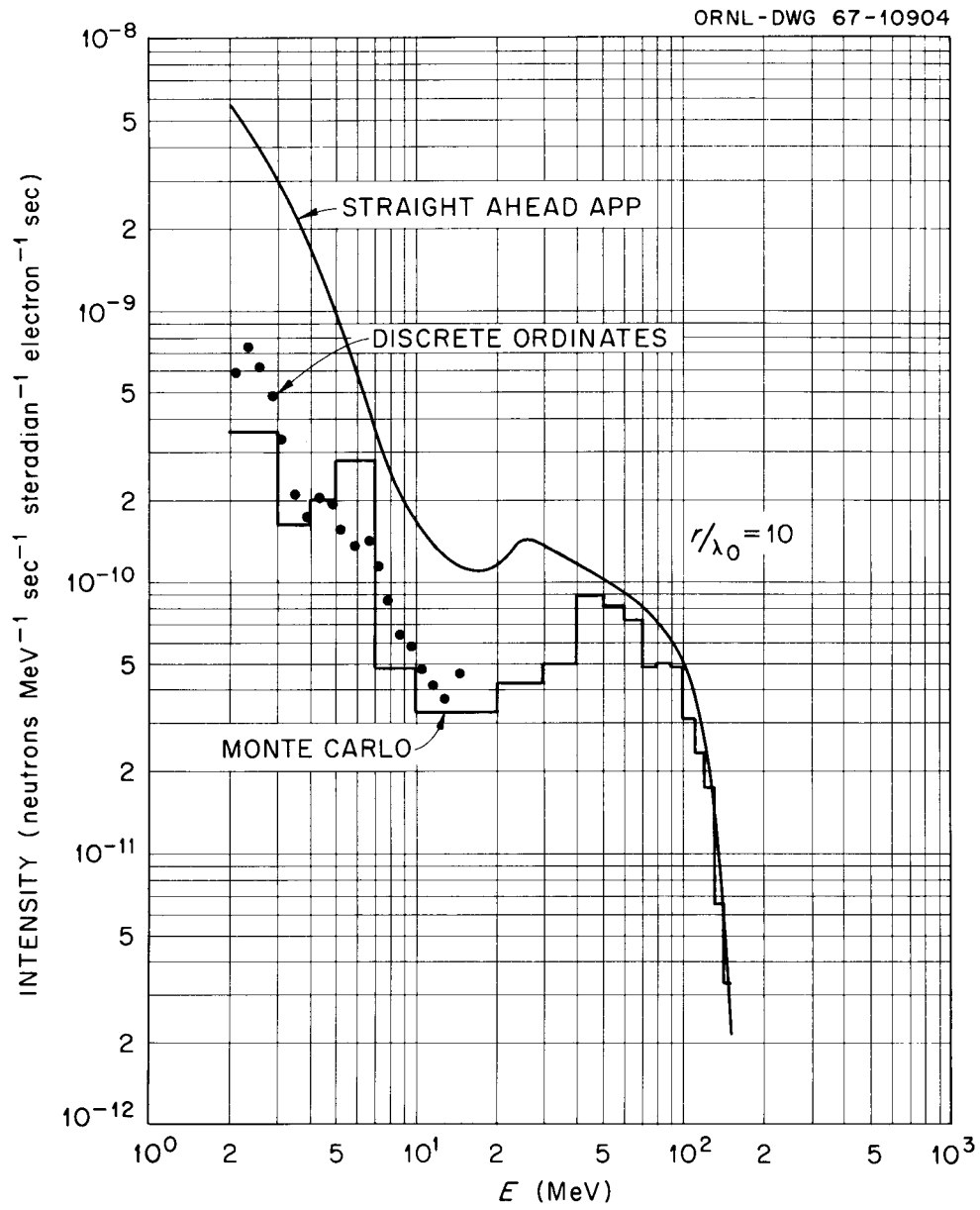


Fig. 7. Neutron Intensity vs Energy Shield Material = SiO<sub>2</sub> with 10% H<sub>2</sub>O.

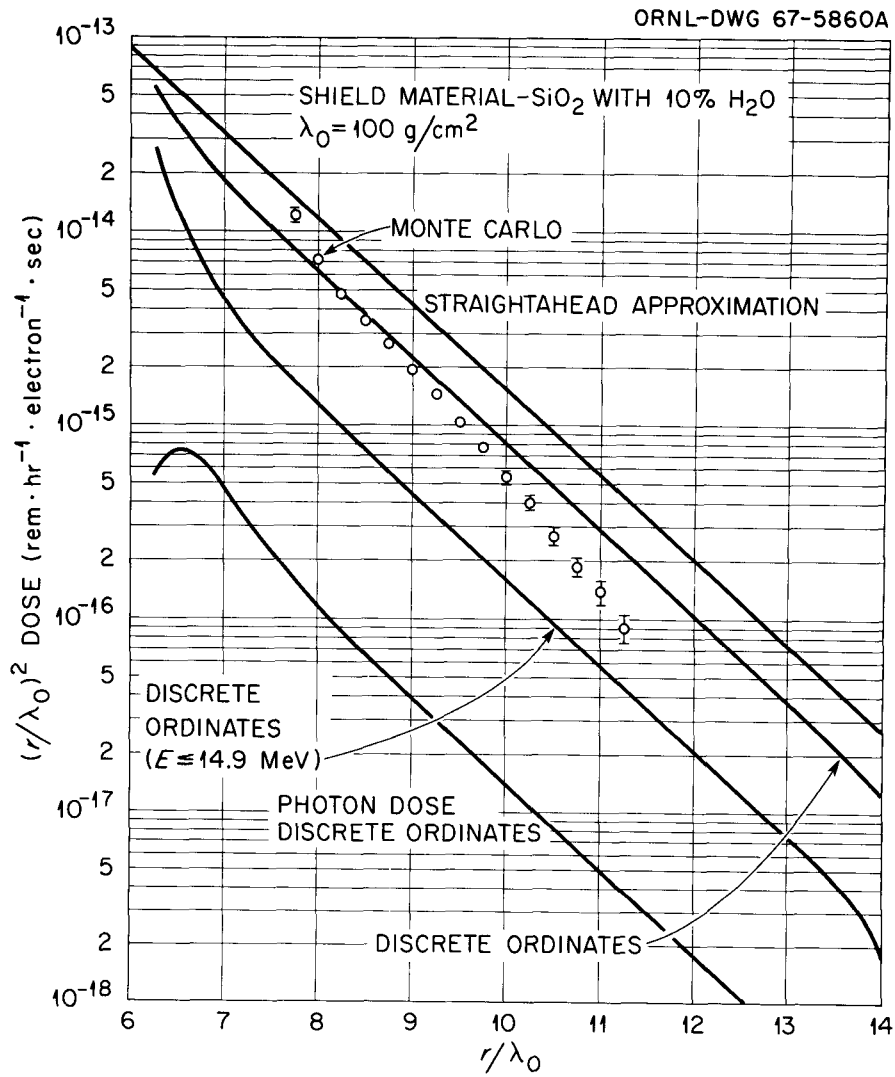


Fig. 8.  $\left(\frac{r}{\lambda_0}\right)^2$  Dose vs Radius.

from 0.01 MeV to thermal energy. The thermal-neutron intensity, as given by the discrete ordinates code in the case of the silicon dioxide shield (see Fig. 3), is approximately  $3 \times 10^{-1}$  neutrons  $\text{MeV}^{-1}$  steradian $^{-1}$  sec $^{-1}$  electron $^{-1}$  sec and in the case of the silicon dioxide and water shield is approximately  $2 \times 10^{-2}$  neutrons  $\text{MeV}^{-1}$  steradian $^{-1}$  sec $^{-1}$  electron $^{-1}$  sec; that is, the thermal intensity is approximately 6 orders of magnitude larger than the intensity at 0.01 MeV at a depth of 1000 g/cm $^2$ .

In Figs. 4 and 7 the neutron intensity calculated using Monte Carlo methods and the straightahead approximation shows a local minimum and maximum in the energy range 10 to 50 MeV. This feature of the intensity arises, at least to some extent, because a different nuclear model is used to calculate particle production from nonelastic collisions above 25 MeV than is used below 25 MeV, and the two models do not agree at 25 MeV. Because of this difficulty with nuclear data, the shape of the spectrum in the energy region must be considered to be very approximate.\*

In Figs. 3, 4, 6, and 7 the intensity calculated in the straightahead approximation is considerably larger at the lower energies than that given by either the discrete ordinates calculation or the Monte Carlo calculation. This overestimate given by the straightahead approximation could presumably be reduced by introducing removal cross sections, that is, by discriminating against particles scattered at large angles, but this has not been done here. The intensities obtained using the discrete ordinates and Monte Carlo methods are in rough agreement, but the discrete ordinates intensity tends to be

---

\* Calculations recently published by K. O'Brien and J. E. McLaughlin<sup>24</sup> in a case similar to those considered here do not give maxima and minima but do give a very flat spectrum in this energy region.

slightly higher than the Monte Carlo intensity at the lower energies ( $\leq 2-3$  MeV). Since the straightahead intensity at the higher energies ( $> 14.9$  MeV) is larger than the Monte Carlo intensity, the source of low-energy ( $< 14.9$  MeV) neutrons that is used in the discrete ordinates calculation is larger than that used in the Monte Carlo calculations, and it is to be expected that the discrete ordinates intensity will be larger than the Monte Carlo intensity at the lower energies. In the method which employs the discrete ordinates code, the only estimate of the intensity above 14.9 MeV is that given by the straightahead approximation. It is to be noted in Figs. 4 and 7 that there is a large difference between the straight-ahead intensity at 14.9 MeV and the discrete ordinates intensity at this energy. This means that the straightahead approximation is not valid at energies as low as 14.9 MeV. It further means that in estimating the dose using the discrete ordinates method as applied here, that is, coupling with the straightahead approximation at 14.9 MeV, one must use an intensity that is discontinuous at 14.9 MeV, and one necessarily obtains an overestimate of the dose from the neutrons with energy greater than 14.9 MeV.\* An estimate of how low in energy the straightahead approximation can reasonably be used may be obtained by comparing the Monte Carlo intensity with the straight-ahead intensity in Figs. 4 and 7. In Fig. 4 the two intensities are in rough agreement for energies greater than 50 MeV, while in Fig. 7 the Monte Carlo intensity is slightly lower than the straightahead intensity at most of the energies shown. On the basis of this somewhat limited amount of information, it would seem that the straightahead approximation can be expected to give reasonable results only for energies of the order of 100 MeV

---

\* The fact that 14.9 MeV was used as the coupling energy was largely a matter of convenience. Given the differential production cross sections, the discrete ordinates code in principle can be used to transport higher energy neutrons.

or more. It must be emphasized, however, that this is not a very firm conclusion because the Monte Carlo calculations have been carried out only over relatively short distances ( $250 \text{ g/cm}^2$  in Figs. 4 and 7), and the error at the higher energies may become more pronounced at larger depths. Furthermore, the energy at which the straightahead approximation becomes valid may depend on geometry and on the energy spectrum of the neutrons in the shield.

In Figs. 5 and 8 the doses obtained in the various approximations are compared. Since in the discrete ordinates method as used here the dose from neutrons with energies greater than  $14.9 \text{ MeV}$  must be obtained from the straightahead approximation, the dose from neutrons with energy less than  $14.9 \text{ MeV}$ , as well as the dose from neutrons with all energies, is shown in the figures. Also shown is the photon dose obtained from the discrete ordinates code. To obtain the total dose the photon dose must be added to the curve labeled "discrete ordinates." In both the discrete ordinates and Monte Carlo calculations the contribution of the thermal neutrons to the dose is included. In the discrete ordinates calculations the contribution of the neutrons with energy less than  $0.4 \text{ eV}$  was obtained separately, and it was found that these neutrons contributed approximately 10% of the dose obtained from all neutrons with energy less than  $14.9 \text{ MeV}$ ; that is, approximately 10% of the dose shown in Figs. 5 and 8 by the curves labeled "Discrete Ordinates ( $E \leq 14.9 \text{ MeV}$ )" is due to neutrons with energy less than  $0.4 \text{ eV}$ . The fact that the neutron dose obtained in the discrete ordinates calculation approaches that given by the straightahead approximation at  $r/\lambda_0 = 6$  and the fact that the neutron dose obtained in the Monte Carlo calculation approaches that given by the straightahead approximation at  $r/\lambda_0 = 7.5$  are a direct consequence of the manner in which the calculations

were done. The rapid variation of the dose at depths just larger than  $r/\lambda_0 = 6$  in the discrete ordinates calculations and  $r/\lambda_0 = 7.5$  in the Monte Carlo calculations is indicative of the fact that the "equilibrium" energy spectrum obtained in the straightahead approximation is very different from the "equilibrium" spectrum obtained in the discrete ordinates and Monte Carlo calculations. The region of rapid variation is larger in the case of the silicon-dioxide shield than in the case of the silicon-dioxide and water shield because the very low energy neutrons come into "equilibrium" very slowly when there is no hydrogen. This is particularly noticeable in the case of the photon dose because the photon production is determined primarily by the capture of the very low energy neutrons. At sufficiently large depths all of the doses have a dependence on depth which is roughly exponential. The observable deviation of the discrete ordinates neutron doses from exponential behavior in the region  $r/\lambda_0 > 13$  is due to the fact that the discrete ordinates calculations were carried out for a finite shield with a maximum  $r/\lambda_0$  of 14. It is significant to note that the neutron dose obtained in the discrete ordinates calculations has essentially the same attenuation length as the dose obtained in the straightahead approximation. To some extent this is to be expected because the neutron source in the discrete ordinates calculation is obtained from the straightahead approximation. The error bars on the Monte Carlo points represent one standard deviation calculated on the basis of batch statistics. In spite of the fact that the error bars on the last few points shown in Figs. 5 and 8 are not large, these points are probably not as statistically reliable as the points at smaller depths. Because of the relatively short distances over which the particles are transported in the Monte Carlo calculations and because of statistical

fluctuations, it is difficult to obtain an accurate attenuation length from the Monte Carlo results. In the silicon-dioxide shield, if one neglects the points at  $r/\lambda_0 \geq 10.75$  as being somewhat unreliable, the attenuation length obtained in the Monte Carlo calculations seems to be roughly comparable to that obtained in the other calculations. In the case of the shield containing silicon dioxide and water, however, the Monte Carlo calculation seems to give an attenuation length which is different from that given by the other calculations. In considering these attenuation results, it must be remembered that the geometry used in the Monte Carlo calculations is not exactly that used in the other calculations and therefore the attenuation length in the Monte Carlo case is not completely comparable to that obtained in the other cases.

Insofar as magnitude is concerned, in both shields the dose obtained in the straightahead approximation is too large. The curves labeled "discrete ordinates" are also too high because they contain an overestimate of the contribution of the neutrons with energy greater than 14.9 MeV. The dose values given by the Monte Carlo calculations, at least at values of  $r/\lambda_0$  sufficiently large compared to 7.5 that equilibrium has been approximately established, are presumably the most correct. The difference between the Monte Carlo doses and the curves labeled "discrete ordinates ( $E < 14.9$  MeV)" is an approximate estimate of the actual contribution of the neutrons with energies greater than 14.9 MeV.

In Fig. 5 the photon dose is small compared to the neutron dose at the larger depths shown in the figure. It must be understood, of course, that over much of the region shown in the figure the photon dose reflects the large overestimate of the neutron flux given by the straightahead approximation and is therefore not meaningful. In Fig. 8 the photon dose is small compared to the neutron dose at all depths. In considering the photon dose, it must be remembered that the contribution from photons produced by non-elastic neutron-nucleus collisions has been neglected and therefore the calculated photon dose is somewhat too small.

## APPENDIX I

In this appendix a few of the details associated with the photoneutron production which are not given by De Staebler are presented.\* If one introduces all of the assumptions of De Staebler, the differential cross section for photoneutron production in the laboratory system from the quasi-deuteron model may be written

$$\left. \frac{d\sigma}{dE d\Omega} \right|_{\text{QD}} = A \frac{\sigma_D(E_\gamma)}{4\pi} \delta[E' - H_D(E_\gamma)] \frac{dE' d\Omega'}{dE d\Omega} , \quad (\text{A.1})$$

where

$A$  = atomic weight

$\sigma_D$  = photodissociation cross section of the deuteron

$E_\gamma$  = laboratory photon energy

$H_D(E_\gamma)$  = kinetic energy of the produced neutron in the center of momentum

$\frac{dE' d\Omega'}{dE d\Omega}$  = Jacobian to transform the differential cross section from the center-of-momentum to the laboratory system

$E', E$  = kinetic energy in the center-of-momentum and laboratory systems, respectively. (Throughout this appendix primes will be used to indicate center-of-momentum quantities.)

In the above the center-of-momentum system is by definition the center-of-momentum system between the photon and quasi-deuteron which is at rest in the laboratory system. The Jacobian in Eq. A.1 may in the usual manner be written as

$$\frac{dE' d\Omega'}{dE d\Omega} = \frac{p}{p'} , \quad (\text{A.2})$$

\*The derivation presented here is due to Dr. F. S. Alsmiller.

where

$p, p'$  = momentum of particle in laboratory and center-of-momentum systems, respectively.

Since in Eq. 3.1 in the text the differential cross section is integrated over  $dE_\gamma$ , it is necessary to rewrite the delta function in Eq. A.1 in a form which is convenient for this integration. This may be done by means of the theorem

$$\delta[f(x)]dx = \frac{\delta(f)}{\left|\frac{df}{dx}\right|} df \quad . \quad (A.3)$$

Thus Eq. A.1 becomes

$$\left.\frac{d\sigma}{dEd\Omega}\right|_{QD} dG_D = A \frac{\sigma_D(E_\gamma)}{4\pi} \frac{p}{p'} \delta(G_D) \frac{1}{\left|\frac{dG_D}{dE_\gamma}\right|} dG_D \quad , \quad (A.4)$$

where

$$G = E' - H(E_\gamma)$$

and, after a trivial change in notation,

$$\left.\frac{d\sigma}{dEd\Omega}\right|_{QD} dE_\gamma = A \frac{\sigma_D(E_\gamma)}{4\pi} \frac{p}{p'} \delta[E_\gamma - I_D] \frac{1}{\left|\frac{dG_D}{dE_\gamma}\right|} dE_\gamma \quad , \quad (A.5)$$

where  $I_D$  is now the value of  $E_\gamma$  such that

$$G_D(E_\gamma) = 0 \quad . \quad (A.6)$$

In a like manner, making all of the assumptions of De Staebler, the differential cross section in the laboratory system for photoneutron production by pion production and reabsorption in the same nucleus may be written

$$\left. \frac{d\sigma}{dE d\Omega} \right|_{\pi} dG_D = \left[ .8A \frac{\sigma_{\pi}(E_{\gamma})}{4\pi} \frac{p_{\pi}}{p'_{\pi}} \delta(G_{\pi}) \frac{1}{\left| \frac{dG_{\pi}}{dE_{\gamma}} \right|} \frac{d\epsilon_{\pi}}{dE} \right]_{\epsilon_{\pi}=2E} dG_D, \quad (\text{A.7})$$

where

$$G_{\pi} = E'_{\pi} - H_{\pi}(E_{\gamma})$$

$\sigma_{\pi}$  = total cross section for pion production from pion-nucleon collision

$p_{\pi}, p'_{\pi}$  = pion momentum in the laboratory and center-of-mass systems, respectively

$H'_{\pi}(E_{\gamma})$  = kinetic energy of the produced pion in the center-of-momentum system

$\epsilon_{\pi}$  = the total energy of the produced pion

and the symbol  $\left[ \quad \right]_{\epsilon_{\pi}=2E}$  means that the pion total energy is to be replaced by two times the neutron kinetic energy. The center-of-momentum system in this case is defined to be the center-of-momentum system between the photon and a nucleon at rest in the laboratory system. Changing variables as before, we have then

$$\left. \frac{d\sigma}{dE d\Omega} \right|_{\pi} dE_{\gamma} = \left[ .8A \sigma_{\pi}(E_{\gamma}) \delta(E_{\gamma} - I_{\pi}) \frac{1}{\left| \frac{dG_{\pi}}{dE_{\gamma}} \right|} \frac{d\epsilon_{\pi}}{dE} \right]_{\epsilon_{\pi}=2E} dE_{\gamma}, \quad (\text{A.8})$$

where  $I_{\pi}$  is the value of  $E_{\gamma}$  such that

$$G_{\pi}(E_{\gamma}) = 0. \quad (\text{A.9})$$

To evaluate the functions occurring in Eqs. A.5 and A.9, consider the process

$$\gamma + S \rightarrow n_A + n_B$$

where if the target S is a quasi-deuteron,  $n_A$  and  $n_B$  are both nucleons, and if the target is a nucleon,  $n_A$  will be taken to be the pion and  $n_B$  will be taken to be the nucleon.

In the laboratory system the total energy  $\epsilon_T$  and momentum  $\vec{P}_T$  may be written before the collision as

$$\vec{P}_T = \vec{p}_\gamma \tag{A.10}$$

$$\epsilon_T = \epsilon_\gamma + \epsilon_S \tag{A.11}$$

and after the collision as

$$\vec{P}_T = \vec{p}_A + \vec{p}_B \tag{A.12}$$

$$\epsilon_T = \epsilon_A + \epsilon_B \tag{A.13}$$

and the velocity of the center-of-momentum  $\vec{\beta}$  may be written

$$\vec{\beta} = \frac{\vec{P}_T}{E_T} \tag{A.14}$$

In the center-of-momentum system

$$\vec{P}'_T = 0 \tag{A.15}$$

$$\epsilon'_T = \epsilon'_\gamma + \epsilon'_S \tag{A.16}$$

before the collision and

$$\vec{P}'_T = 0 \tag{A.17}$$

$$\epsilon'_T = \epsilon'_A + \epsilon'_B \tag{A.18}$$

after the collision. The invariant mass  $m_T$  is given by

$$m_T = \sqrt{\epsilon_T^2 - p_T^2} = \epsilon_T' . \quad (\text{A.19})$$

In the laboratory system

$$\begin{aligned} m_T &= \sqrt{(E_\gamma + m_S)^2 - p_\gamma^2} \\ &= \sqrt{m_S^2 + 2E_\gamma m_S} , \end{aligned} \quad (\text{A.20})$$

while in the center-of-momentum system

$$m_T = \sqrt{\epsilon_A'^2 + \epsilon_B'^2} , \quad (\text{A.21})$$

and, after some algebra,

$$p_A'^2 = p_B'^2 = \frac{(m_A^2 + m_B^2 - m_T^2)^2}{4m_T^2} - \frac{m_A^2 m_B^2}{m_T^2} \quad (\text{A.22})$$

$$\epsilon_A' = \frac{m_T^2 + m_A^2 - m_B^2}{2m_T} \quad (\text{A.23})$$

$$\epsilon_B' = \frac{m_T^2 + m_B^2 - m_A^2}{2m_T} . \quad (\text{A.24})$$

Furthermore, from the Lorentz transformation we have

$$\epsilon_A' = \gamma_{\text{CM}} [\epsilon_A - \beta_{\text{CM}} \cdot \vec{p}_\pi] ,$$

so

$$\epsilon_A' = \frac{\epsilon_\gamma + \epsilon_S}{m_T} \left[ \epsilon_A - \frac{\vec{p}_\gamma \cdot \vec{p}_A}{\epsilon_\gamma + \epsilon_S} \right] \quad (\text{A.25})$$

and

$$G = \frac{(\epsilon_\gamma + \epsilon_S) \epsilon_A}{m_T} - \frac{\vec{p}_\gamma \cdot \vec{p}_A}{m_T} - \frac{m_T^2 + m_A^2 - m_B^2}{2m_T} . \quad (\text{A.26})$$

The value of the photon energy for which  $G(E_\gamma)$  is zero is from Eq. A.26:

$$\epsilon_\gamma = \frac{\epsilon_A \epsilon_S - \frac{1}{2}(m_S^2 + m_A^2 - m_B^2)}{p_A \cos\theta - \epsilon_A + m_S}, \quad (\text{A.27})$$

where

$\cos\theta$  = the cosine of the angle between the momentum of particle A in the laboratory system and the incident photon direction.

Because of the delta function in Eqs. A.5 and A.8, we shall be interested in the quantity  $\frac{p}{p'} \left[ \frac{dG}{dE_\gamma} \right]$  evaluated at the zero of the delta function, that is, at the value of  $E_\gamma$  given by Eq. A.27. It will be convenient to express the various quantities in terms of the invariant mass  $m_T$ , so for future reference we note

$$m_T \Big|_{G=0} = \left\{ m_S^2 + 2m_S \frac{[\epsilon_A \epsilon_S - \frac{1}{2}(m_S^2 + m_A^2 - m_B^2)]}{p_A \cos\theta - \epsilon_A + m_S} \right\}^{\frac{1}{2}}. \quad (\text{A.28})$$

Also,

$$\frac{d(m_T G)}{dE_\gamma} = m_T \frac{dG}{dE_\gamma} + G \frac{dm_T}{dE_\gamma} \quad (\text{A.29})$$

so

$$\frac{dG}{dE_\gamma} \Big|_{G=0} = \left[ \frac{1}{m_T} \frac{d(m_T G)}{dE_\gamma} \right]_{G=0} \quad (\text{A.30})$$

and, from Eq. A.26,

$$\frac{dG}{dE_\gamma} \Big|_{G=0} = \frac{\epsilon_A - p_A \cos\theta - m_S}{m_T \Big|_{G=0}}. \quad (\text{A.31})$$

Now, using Eqs. A. 22, A.28, and A.31, the quantity  $\left[ \frac{p}{p'} \left[ \frac{dG}{dE_\gamma} \right] \right]_{G=0}$  can be evaluated explicitly.

In the case of the deuteron model,

$$\epsilon_S = 2m \quad , \quad (\text{A.32})$$

where

$m$  = nucleon mass,

so (going to kinetic energies) from Eq. A.27

$$I_D = \frac{2mE}{\cos\theta\sqrt{E(E+2m)} - E + m} \quad , \quad (\text{A.33})$$

and from Eq. A.28

$$m_T|_{G=0} = 2m \left\{ 1 + \frac{2E}{\cos\theta\sqrt{E(E+2m)} - E + m} \right\}^{1/2} \quad . \quad (\text{A.34})$$

From Eq. A.31

$$\left. \frac{dG}{dE_\gamma} \right|_{G=0} = \frac{E - \cos\theta\sqrt{E(E+2m)} - m}{m_T|_{G=0}} \quad , \quad (\text{A.35})$$

and from Eq. A.22

$$\begin{aligned} p'|_{G=0} &= \left[ \frac{m_T^2|_{G=0}}{4} - m^2 \right]^{1/2} \\ &= \left[ \frac{2m^2E}{\cos\theta\sqrt{E(E+2m)} - E + m} \right]^{1/2} \quad . \end{aligned} \quad (\text{A.36})$$

Combining these results we have finally

$$J_D(E, \cos\theta) = \left[ \frac{p}{p'} \frac{1}{\left| \frac{dG}{dE_\gamma} \right|} \right]_{G=0} = \sqrt{2} \frac{\sqrt{E(E+2m)}}{\sqrt{E}} \frac{[\cos\theta\sqrt{E(E+2m)} + E + m]^{1/2}}{\cos\theta\sqrt{E(E+2m)} - E + m} \quad , \quad (\text{A.37})$$

and then Eqs. A.5, A.33, and A.37 give explicitly Eq. 3.3 of the text.

In the case of pion production and reabsorption,

$$\begin{aligned}\epsilon_S &= m \\ m_A &= m_\pi \\ m_B &= m \quad ,\end{aligned}\tag{A.38}$$

so from Eq. A.27

$$I_\pi = \frac{\epsilon_\pi \cdot m - \frac{1}{2} m_\pi^2}{\cos\theta \sqrt{\epsilon_\pi^2 - m_\pi^2} - \epsilon_\pi + m} \quad ,\tag{A.39}$$

and from Eqs. A.22 and A.31

$$p_A \Big|_{G=0} = \frac{[m^2 I_\pi^2 - m m_\pi^2 I_\pi + \frac{1}{4} m_\pi^4 - m_\pi^2 m^2]^{\frac{1}{2}}}{[m(2 I_\pi + m)]^{\frac{1}{2}}}\tag{A.40}$$

$$\frac{dG}{dE} \Big|_{\gamma G=0} = \frac{\epsilon_\pi - \cos\theta \sqrt{\epsilon_\pi^2 - m_\pi^2} - m}{[m(2 I_\pi + m)]^{\frac{1}{2}}}\tag{A.41}$$

Combining these equations and evaluating the result at  $\epsilon_\pi = 2E$ , we have

$$J_\pi(E, \cos\theta) = \left[ \frac{p}{p' \left| \frac{dG}{dE} \right|} \right]_{\substack{G=0 \\ \epsilon_\pi = 2E}} = \frac{2\sqrt{(2E+m_\pi)(2E-m_\pi)}}{Q(I_\pi) [\cos\theta \sqrt{(2E+m_\pi)(2E-m_\pi)} - 2E+m]} \tag{A.42}$$

$$Q(I_\pi) = \frac{[m^2 I_\pi^2 - m m_\pi^2 I_\pi - m_\pi^2 m^2 + \frac{1}{4} m_\pi^4]^{\frac{1}{2}}}{m(2I_\pi + m)} \quad ,$$

and then Eqs. A.8, A.39, and A.42 give explicitly Eq. 3.4 in the text.

## REFERENCES

1. C. D. Zerby and H. S. Moran, "Studies of the Longitudinal Development of High-Energy Electron-Photon Cascade Showers in Copper," ORNL-3329 (1962).
2. C. D. Zerby and H. S. Moran, "A Monte Carlo Calculation of the Three-Dimensional Development of High-Energy Electron Photon Cascade Showers," ORNL-TM-422 (1962).
3. C. D. Zerby and H. S. Moran, Neutron Phys. Div. Ann. Progr. Rept. Aug. 1, 1963, ORNL-3499, Vol. II, p. 3.
4. B. Rossi, *High-Energy Particles*, Prentice-Hall, Inc., Englewood Cliffs, N. J., 1956, p. 244.
5. J. S. Levinger, *Nuclear Photo-Disintegration*, Oxford Univ. Press, Oxford, London, 1960.
6. D. N. Olson, "Photoprotons from Nuclei Exposed to 1 BeV Bremsstrahlung Radiation," Thesis, Cornell University, Ithaca, N. Y., 1960 (unpublished).
7. H. De Staebler, Jr., "Transverse Radiation Shielding for the Stanford Two-Mile Accelerator," Stanford Linear Electron Accelerator Center, SLAC 9 (1962).
8. J. L. Matthews, "Calculation of Nucleon Spectra and Angular Distributions from the Quasi-Deuteron Model for the High-Energy Photoeffect," Massachusetts Institute of Technology (to be published).
9. J. L. Matthews, "Notes on a Comparison of a Quasi-Deuteron Model for High-Energy Photoproton Spectra with Some Experimental Data," Massachusetts Institute of Technology, LNS Report 110 (1966).
10. H. Bertini, Nucl. Phys. 87, 138 (1966).

11. R. G. Alsmiller, Jr., *et al.*, "Analytic Representation of Nonelastic Cross Sections and Particle-Emission Spectra from Nucleon-Nucleus Collisions in the Energy Range 25 to 400 MeV," ORNL-4046 (1967).
12. D. C. Irving. The master cross-section tape for use in the O5R Monte Carlo code, as well as references to all the data used, is available on request from the Radiation Shielding Information Center of the Oak Ridge National Laboratory.
13. H. Bertini, "Monte Carlo Calculations on Intranuclear Cascades," ORNL-3383 (1963).
14. L. Dresner, "EVAP - a Fortran Program for Calculating the Evaporation of Particles from Excited Compound Nuclei," ORNL-TM-196 (1961).
15. R. G. Alsmiller, Jr., "Nucleon-Nucleus and Pion-Nucleus Collisions in the Energy Range 2 to 10 GeV," ORNL-3855 (1965), Appendix 1.
16. W. W. Engle, Jr., "A Users Manual for ANISN, A One-Dimensional Discrete Ordinates Transport Code with Anisotropic Scattering," Computing Technology Center, Union Carbide Corporation, Oak Ridge, Tenn., K-1693 (1967).
17. G. D. Joanou and J. S. Dukek, "GAM II, A B3 Code for the Calculation of Fast Neutron Spectra and Associated Multigroup Constants," GA-4265 (1963).
18. *Reactor Handbook, Vol. III, Part B, Shielding*, ed. E. P. Blizard and L. S. Abbott, Interscience Publishers, New York, 1962.
19. W. E. Kinney, "The Nucleon Transport Code, NTC," ORNL-3610 (1964).
20. *Protection Against Neutron Radiation up to 30 Million Electron Volts*, National Bureau of Standards Handbook 63 (1957).
21. D. C. Irving *et al.*, Nucl. Instr. Methods 51, 129 (1967).

22. C. D. Zerby and W. E. Kinney, Nucl. Instr. Methods 36, 125 (1965).
23. B. J. Henderson, "Conversion of Neutron or Gamma Ray Flux to Absorbed Dose Rate," Radiation Shielding Course, Oak Ridge School of Reactor Technology, 1959 (unpublished).
24. K. O'Brien and J. E. McLaughlin, "The Propagation of the Neutron Component of the Nucleonic Cascade at Energies Less Than 500 MeV: Theory and A Solution to the Accelerator Transverse Shielding Problem," HASL Technical Memorandum 67-9 (1967).

## INTERNAL DISTRIBUTION

- |                                     |                                 |
|-------------------------------------|---------------------------------|
| 1. Biology Library                  | 149. F. F. Haywood              |
| 2-4. Central Research Library       | 150. F. T. Howard               |
| 5-6. ORNL - Y-12 Technical Library  | 151. Troyce Jones               |
| Document Reference Section          | 152. W. H. Jordan               |
| 7-96. Laboratory Records Department | 153. C. E. Larson               |
| 97. Laboratory Records, ORNL R.C.   | 154. H. G. MacPherson           |
| 98. L. S. Abbott                    | 155-156. F. C. Maienschein      |
| 99-128. R. G. Alsmiller             | 157. B. F. Maskewitz            |
| 129. T. W. Armstrong                | 158. J. G. Sullivan             |
| 130. H. W. Bertini                  | 159. D. A. Sundberg             |
| 131-135. J. Barish                  | 160. A. M. Weinberg             |
| 136. C. E. Bettis                   | 161. G. Dessauer (consultant)   |
| 137-141. R. T. Boughner             | 162. B. C. Diven (consultant)   |
| 142. C. E. Clifford                 | 163. W. N. Hess (consultant)    |
| 143-147. W. W. Engle                | 164. M. H. Kalos (consultant)   |
| 148. J. A. Harvey                   | 165. L. V. Spencer (consultant) |

## EXTERNAL DISTRIBUTION

166. P. B. Hemmig, Division of Reactor Development and Technology,  
U.S. Atomic Energy Commission, Washington, D.C.
167. I. F. Zartman, Division of Reactor Development, U.S. Atomic  
Energy Commission, Washington, D.C.
168. J. A. Swartout, Union Carbide Corporation, New York
169. Laboratory and University Division, AEC, ORO
- 170-483. Given distribution as shown in TID-4500 under Physics category  
(25 copies - CFSTI)